Soft microflow sensors†

Rafaele Attia,[a] Daniel C. Pregibon,[b] Patrick S. Doyle,[b] Jean-Louis Viovy[a] and Denis Bartolo[c]

Received 8th August 2008, Accepted 13th January 2009
First published as an Advance Article on the web 12th February 2009
DOI: 10.1039/b813860e

We present a rapid prototyping method for integrating functional components in conventional PDMS microfluidic devices. We take advantage of stop-flow lithography (D. Dendukuri, S. S. Gu, D. C. Pregibon, T. A. Hatton and P. S. Doyle, *Lab Chip*, 2007, **7**, 818)[1] to achieve the *in situ* fabrication of mobile and deformable elements with a controlled mechanical response. This strategy is applied to the fabrication of microflow sensors based on a deformable spring-like structure. We show that these sensors have a large dynamic range, typically 3 to 4 orders of magnitude, and that they can be scaled down to measure flows in the nl per min range. We prepared sensors with different geometries, and their flow-elongation characteristics were modeled with a simple hydrodynamic model, with good agreement between model and experiments.

Introduction

Beyond miniaturization and reduction of reagents consumption, one of the major advantages of microfluidics is the possibility to fully integrate biological or chemical processes in a single device without the requirement of expensive and cumbersome robotics (sample-to-result strategy).[2] This lab on a chip approach requires the integration in a single chip of various functional components, such as valves, pumps, mixers, sensors and analyzers. Silicon "hard" lithography is the most common approach to microfabricate and integrate functional structures, such as MEMS.[3] This technology can yield mobile structures with high spatial resolution (below 1 μm) and reproducibility. Important examples are micro-cantilevers for environmental, chemical and biological detection,[4,5] membranes micropumps,[6] and electrostatic rotary motors.[7] However the multi-step techniques used to develop these components are highly time-consuming and require specialized clean room equipment. Several days to several weeks are typically required, making these methods inappropriate for laboratory prototyping and small production series. Moreover, the conventional materials involved in MEMS technologies have a large elastic modulus, allowing for weak deformations only. Finally, their chemical properties are usually not compatible with biological processes, unless specific surface modifications are performed.

Recently, a few alternative strategies have been proposed to achieve rapid prototyping of integrated functional components. Simms *et al.*[8] proposed a promising method, also based on a sequential lithography and etching process but involving polymeric materials. This method does not require expensive and specialized equipment, but it is so far limited to millifluidic applications with typical minimal sizes in the 100 μm–1 mm range. Beebe and coworkers[9] have proposed a very simple and elegant method to fabricate microstructures by *in situ* photolithography of acrylic polymer gels, demonstrating for instance the fabrication of pH sensitive microvalves in millifluidic channels. This single step process is fast and easy to implement. The integrated gel based components are deformable, but they cannot freely move in the channel (they are bound to the walls), and the typical time constant of actuation by gel swelling is rather long. Another limitation of this strategy is that pH is a critical parameter for many biological applications, so it is not always possible to use this property as a flow-control parameter. As for the technology proposed in ref. 8 the typical size of the photopolymerized valves described in ref. 9 is in the millifluidic range.

In this paper, we show how to take advantage of continuous flow lithography,[10] a high-throughput technique recently proposed for the fabrication of microparticles, to easily include mobile and deformable "soft MEMS" inside PDMS microchannels. The main idea underlying this approach is to shape a photopolymerizable polymer flown in a microchannel, by microscope projection photolithography. The functional component is thus fabricated *in situ*, which simplifies greatly the process of integrating and aligning soft-MEMS inside microfluidic circuits.

The use of polymer-based materials enables the fabrication of soft structures with elastic moduli typically six orders of magnitude smaller than that of silicon used in conventional MEMS. These structures also have a considerably larger range of reversible elastic deformation. In addition, the free radical photopolymerization process yields hanging structures free to move in the microchannel, without dealing with complex sacrificial layers. Stop-flow lithography allows for the preparation of various designs in a matter of minutes, offering unprecedented versatility for the testing of integrated mechanical elements.

---

[a] *Laboratoire Physicochimie Curie, CNRS/UMR 168, 11 rue Pierre et Marie Curie, Paris, France. E-mail: rafaele.attia@curie.fr; jean-louis.viovy@curie.fr; Fax: (+33) 1 40 51 06 36; Tel: (+33) 1 56 24 68 44*

[b] *Department of Chemical Engineering, Massachusetts Institute of Technology, 77 Massachusetts Ave., Cambridge, MA, 02139, USA. E-mail: pregibon@mit.edu; pdoyle@mit.edu*

[c] *PMMH laboratory ESPCI-CNRS UMR 7636-Université Paris 6-Université Paris 7, 10, rue Vauquelin, 75231 Paris cedex 05, France. E-mail: denis.bartolo@espci.fr*

† Electronic supplementary information (ESI) available: Relative extension *versus* NQ for different numbers of turns (N = 3, 5, 7 and 9 turns). See DOI: 10.1039/b813860e

Finally, it does not require high resolution tools or masks or any specific clean room equipment. It is thus particularly well adapted to laboratory fast prototyping, and low-cost production of small series.

As a first step toward highly-integrated soft-MEMS design, we demonstrate here the fabrication of in-channel spring-like microflow sensors, and study their characteristics. These flow sensors do not require the addition of specific components in the fluid as microparticles (as used *e.g.* for flow measurement based on particle tracking velocimetry),[11] salt (for electrokinetic detectors),[12] or electrochemically-responsive molecules.[13] As we shall see below, they can also offer a large dynamic range.

Fast integration of soft mobile component in microfluidic devices

Microscope-based projection lithography method

Our microfabrication strategy relies on microscope-based projection lithography. This method only requires a UV lamp, a PDMS microchannel and a microscope objective (Fig 1). For convenience, we used here an inverted microscope. The prepolymer solution is introduced in the microchannel with a syringe pump. The flow is then stopped and focus is precisely made on the bottom surface of the microchannel. Subsequently, the prepolymer is exposed to UV light through a mask located at the field stop position. The exposure time (typically a few tenths of a second) is precisely set thanks to a computer-controlled shutter. As a result, we obtain a solid lithographically defined object. The object size is smaller than the feature on the mask. The reduction factor corresponds to the ratio of the magnification of the microscope objective over the magnification of the tube lens of the microscope. With simple, low-cost dot-printed masks, the size of the functional element can be varied from 1 micrometer, with a high magnification objective (100×), to 10 millimeters, with a low magnification objective (4×). Whatever the chosen shape, the sides of the polymerized structures are essentially parallel to the UV beam direction. Aspect ratios up to 10 : 1 can be easily achieved with low numerical aperture objectives. Importantly, the microfabricated elements do not adhere to the channel walls. This is due to the high permeability of PDMS to gases. Oxygen diffuses rapidly into the prepolymer solution near the PDMS walls, inhibiting free radical in a thin layer (few microns), in which the prepolymer remains uncured. This prepolymer (or the suspending liquid if the channel is flushed by another fluid after polymerization) lubricates the contact between the cross-linked objects and the PDMS walls.[14] Hence, the cross-linked structures are free to move and to deform. In the present application, in order to keep one end of the sensor at a fixed position in the channel, we photopolymerize an anchoring loop around a post integrated at a predefined position in the PDMS microchannel during its fabrication. The loop is centered on the post prior to photopolymerization (see Fig. 2). In order to demonstrate the versatility of the method, we developed several spring-like deformable elements of different geometries (Fig. 1 and 2). The final geometry adopted in the experiments is represented in Fig. 2: The “ball” in Fig. 1 was initially added to stabilize the spring, but in practice deformation was very stable even in the absence of it, and it was removed in subsequent experiments.

In our experiments, we mostly used polyethyleneglycol diacrylate (PEGDA). These acrylate-based polymers are highly reactive and form tightly cross-linked networks upon free radical polymerization. The “softness”, or more precisely the elastic modulus, of the resulting material can be easily and finely tuned by changing the monomer to cross-linker ratio or by lowering the photoinitiator concentration. Moreover, PEGDA polymers combine numerous advantages for biological applications: they

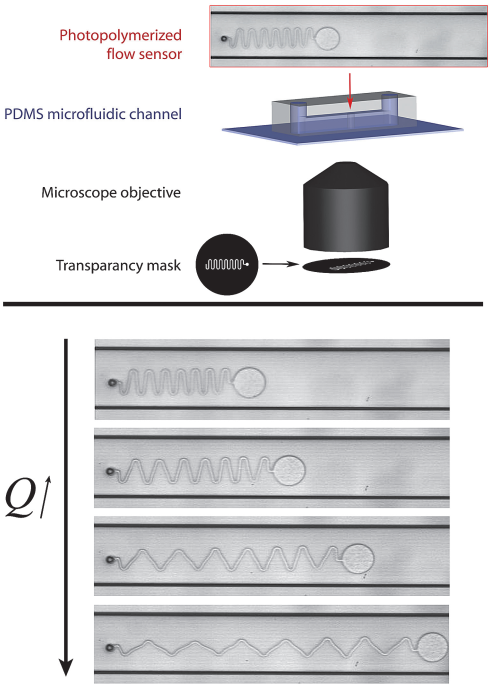

Fig. 1 Top: Schematics of the experimental set-up. A printed mask is placed in the microscope focal plane in order to texture the UV illumination and photopolymerize a resin (PEGDA) with the desired shape. Bottom: Deformation of the photopolymerized spring-shaped component upon flow rate increase. The oxygen inhibition layer in the vicinity of the PDMS surfaces enables the PEGDA microspring to deform freely in the channel. Channel width: 500 μm.

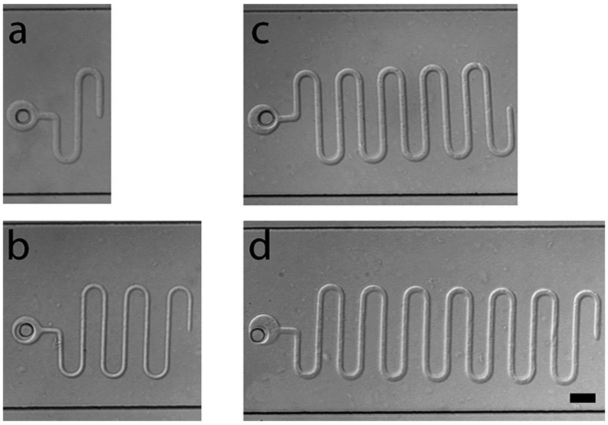

Fig. 2 Pictures of four different PEGDA microspring flow sensors (width 13 μm). a: 1 turn, b: 3 turns c: 5 turns, and d: 7 turns. Scale bars: 100 μm.

have a low swelling ratio in water, they display excellent biocompatibility and biofouling properties, and they are known to reduce non-specific adsorption of biomolecules or cell adhesion.[15] However, the stop-flow lithography strategy can be applied to a wide range of materials with different chemical and physical properties, provided the pre-polymer solution does not appreciably swell PDMS. Depending on the material used as a substrate, the patterned object can be either a resin or a hydrogel.

Soft flow sensor characterization

We now focus on a specific example of integrated functional element. Cross-linked PEGDA networks can reversibly undergo large deformations. We take advantage of this important property to construct spring-like flow sensors with a high range of operation. The spring has the shape of a folded ribbon with a 200 µm width. Its length at rest depends on the number of turns in the spring, and the height is set by the channel height. This height has been measured using a profilometer and was found to be 10 µm. A 70 µm circle at one end is used as an anchor, (Fig. 2). The spring is thus immobilized in the microchannel at one end, and free to deform and move everywhere else. Springs with various numbers of turns N and different thicknesses w were prepared and characterized (N = 3, 5, 7 and 9 turns, w = 9, 13, 16 and 22 µm). Just after polymerization, a constant flow rate is imposed to the PEGDA solution in the 4 cm × 500 µm × 20 µm channel. For the different flow rates, we took pictures of the spring and measured its elongation. Fig. 3 displays the length obtained for a spring with 7 turns, upon repeated cycling of the flow. Deformation was measurable, reproducible and reversible over typically 3 orders of magnitude of flow rate, for more than 200 cycles. In Fig 4, we plot the data obtained for a spring with different thicknesses, over 4 orders of magnitude of flow rate Q, within the range of 10 nl/min to 1 ml/min (the range available to our syringe pump). At low Q, the total relative extension first increases linearly with the flow rate. At high flow rate the total elongation tends to saturate to a constant value, which depends on the spring geometry. To better understand this non-linear response, we investigated the evolution of relative extension amplitude along the flow sensor. The deformation is essentially localized at the "hinges" of the spring, (Fig. 1). It is reflected by a progressive orientation of the spring's linear segments along the flow direction, which provides the essential contribution to changes in the end-to-end distance of the spring. The elongation of each "turn" of the spring (combination of one hinge and the two adjacent half-segments) in the flow direction is plotted in Fig. 5. Turns closer to the attachment point are the most deformed and they also are the first to reach a saturation of their elongation. This saturation progressively extends towards the free end. At small flow rates, the relative extension (projected onto the flow direction) increases linearly with Q for each turn. The slope of this relative extension change increases with the turn index (from the anchor to the end). Indeed, each turn is subject to a stretching force equal to the sum of all viscous forces received by the turns downstream to it. This linear regime crosses over to a saturation regime, corresponding to a full alignment of the turn's straight section in the flow direction. When this happens, the segments are essentially aligned with the flow, and cannot yield any further elongation. This saturation is reached earlier by turns close to the anchoring point, because the force is higher there. The distribution of these saturation points contributes to smoothen the elongation profile, and to increase significantly the dynamic range of the flow sensor. We checked that all the turns in the spring have the same mechanical properties. To do so, we

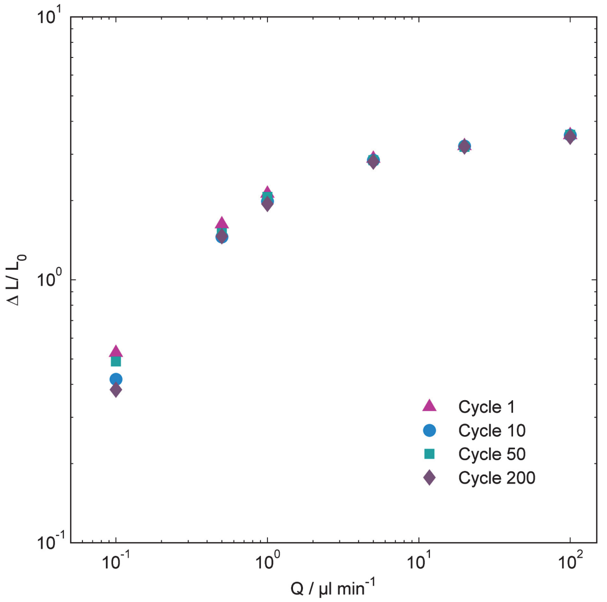

Fig. 3 Flow cycling experiments. The overall relative extension of a microspring composed of 7 turns (w = 13 µm) is plotted at different flow rates. The experiment is repeated 200 times. Triangles: first cycle, circles: 10th cycle, squares: 50th cycle and diamonds 200th cycle.

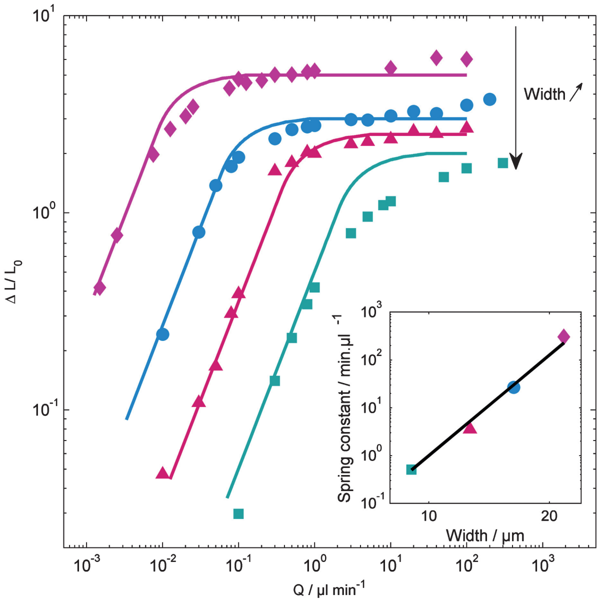

Fig. 4 Relative extension *versus* flow rate for 4 different spring-like flowmeters. The springs are made of 7 turns. Squares: width w = 9 µm, triangle: width w = 13 µm, circle: w = 16 µm, diamonds: w = 22 µm. Insert: The spring constant (defined as the slope of the relative extension *versus* flow rate curves at low Q) is plotted as a function of the spring width in a linear/log scale (squares). It shows a good agreement with a w^7 power law (line).

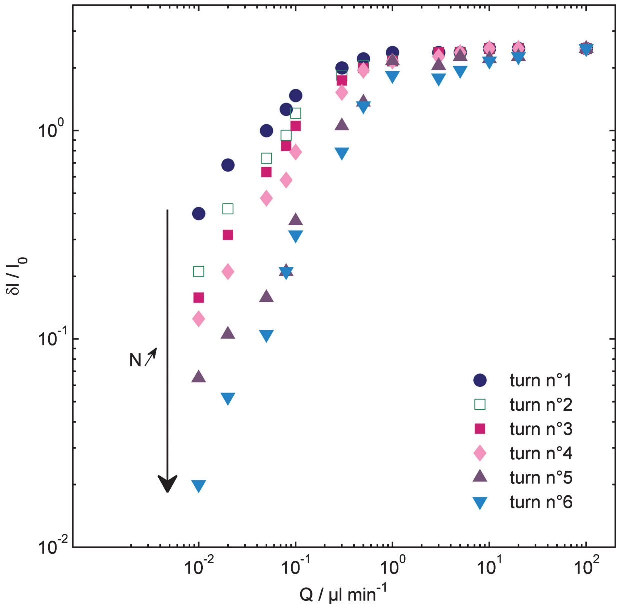

Fig. 5 Local relative extension *versus* flow rate for each turn along a 7 turns spring-shaped flow sensor, $w = 13$ µm. The first turn is the closest to the attachment point.

showed that the flow-elongation characteristics of all segments collapse on a single master curve for microsprings with different N (ESI Fig. S1†).

Modeling

To account for the measured flow-elongation characteristics of the microsprings, we propose a simplified beads and springs model. Each turn of the flow sensor is modelled by a bead connected to a frictionless spring of stiffness k and having a finite extension. In the model, the elongation δl of each connecting spring is supposed to increase linearly with the applied force until it reaches its maximal value δl_{max}, and then remains constant. On top of the associated elastic force, each bead experiences a viscous friction force ξQ. Contrary to the spring stiffness k, the precise value of the friction coefficient ξ is difficult to estimate. It is proportional to the fluid viscosity, but its precise value depends both on the spring shape and on the channel geometry. The total elongation of a spring composed of N turns is readily obtained by summing the relative extension of the N turns. In the linear regime, these relative extensions are deduced from the force balance between elastic and viscous forces, this yields

$$\Delta L = \frac{N(N+1)}{2}\frac{\xi}{k}Q \tag{1}$$

This linear regime ends when the first turn saturates and reaches its maximal elongation (*i.e.* $\delta l = \delta l_{max}$). We are thus left with a spring made of (N–*1*) turns attached to a rigid segment, the total elongation of which is given by the above formula replacing N by N–*1*. For a given Q, we computed the total elongation by iterating this elementary algorithm. When all the turns are fully elongated, the non-linear regime ends by a constant plateau value. This model involves two independent parameters. We extracted (ξ/k) from the linear fit of the experimental curve at low deformations, and kept δl_{max} as a free fitting parameter. The model's prediction is compared with 4 different experiments corresponding to four different spring geometries. As shown in Fig. 4, this crude model is in very reasonable agreement with the experiments. Note that the elongation δl is modeled by a simple linear approximation until full saturation, so our model should overestimate the spring's length in the crossover region between the linear and the saturated regime. Conversely, even after full alignment in the flow direction, the straight sections of the spring can undergo an elongational elastic deformation (stretching), which is not taken into account in the model. Thus, the model should underestimate the spring's elongation at very high flow rate. Combining these two effects, we expect that the real length increase should be more progressive than predicted at high flow rates, which is indeed observed.

Range of operation: lowest measurable flow rate and dynamic range

In order to increase the range of measurable flow rates we investigated the geometrical factors that modify the overall spring constant of the flow sensor. The overall spring constant is proportional to the bending modulus of the hinges, which can be easily tuned by changing the thickness of the spring. The slopes of the linear segments at low Q in Fig. 4 follow a w^7 scaling law, as depicted in Fig. 4 inset. This strong variation demonstrates that changing the spring thickness (by a change in the mask) is an efficient strategy to modulate the range of operation of the flow sensor over several decades. It is worth noticing that the overall spring constant cannot be varied over such a wide range by adjusting the exposure time or the polymer elastic modulus. Moreover, a change in the mask design does not require any extra fine tuning of the polymerization parameters or of the material formulation.

Furthermore, according to eqn. (1), the sensitivity of this flow sensor increases linearly with the number of turns N. In other words, if the smallest measurable deformation is ($\Delta L/L$)min, the minimal flow rate that can be measured by the flow sensor decreases with N and scales as $\sim$($\Delta L/L$)min/(N + 1). Thus, the minimal measurable flow rate can be reduced by sequentially adding turns to an existing spring.

High robustness

These photopolymerized flow-sensors have a high mechanical and chemical robustness. Firstly, we never observed any fatigue effect upon flow cycling experiments. Even after 200 flow rate cycles the spring deformations proved to be reversible, with an error which decreases with the flow rate and which is 15% for 0.1 µl/min and <5% for flow rates above 0.5 µl/min (see Fig. 3) Secondly, the springs deformation is highly reproducible from one spring to another (error<5%) and it remains reversible over a large dynamic range of flow rates, typically 4 orders of magnitude. We were indeed limited here by the dynamic range of our syringe pump, and not by any apparent degradation in the spring's response.

Eventually, measurements were performed both in prepolymer solution or in water, and after different exposure times. Rescaling the flow rate by the fluids shear viscosity, the elongation

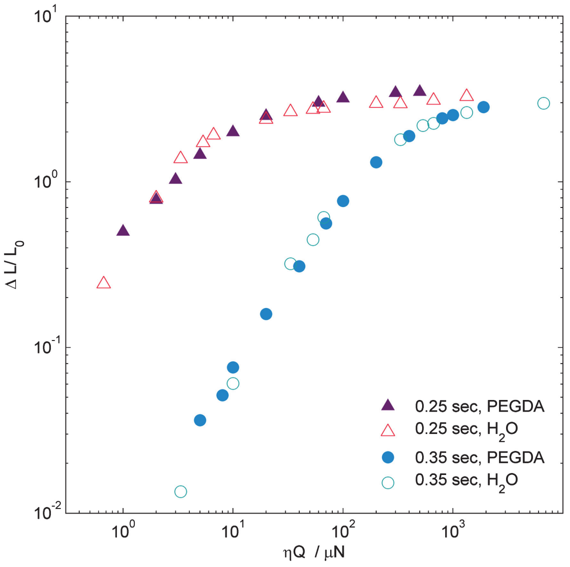

Fig. 6 Relative extension *versus* normalized flow rate curves in water (filled symbols) and liquid PEGDA (empty symbols). The flow rate is renormalized by the viscosity (η) of water or PEGDA. Two springs were made with two different UV exposure times: 0.25 s (triangles) and 0.35 s (circles).

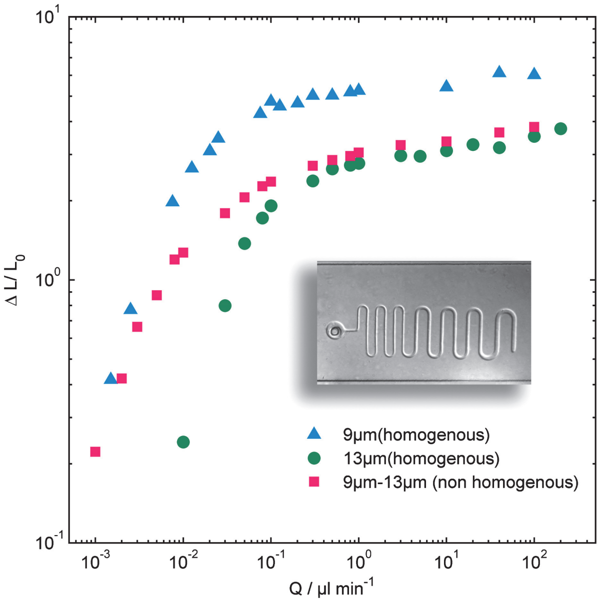

Fig. 7 Relative extension *versus* flow rate for 2 springs with homogenous widths ($w = 9$ and $w = 13$ μm), and for one spring, shown in the picture, with non-homogenous turns width. Half of the turns have a 9 μm width and the second half a 13 μm width.

versus flow rate curves perfectly collapse on the same master curves, (Fig. 6). This demonstrates that the elastic properties of the sensors, and thus their response, were not affected by this exchange between two solvents with very different viscosities and polarities. This suggests that, if some residual swelling of the PEGDA flow sensors exists in water, it does not appreciably modify its mechanical response, and that these sensors should be usable with high accuracy with a high variety of water-based liquids encountered in biological assays.

Toward shape optimization: Non-homogenous spring

As shown in the previous section, the measurable flow rate range is highly related to the spring geometry. Increasing the spring thickness increases the bending modulus and the measurable flow rate range is shifted to higher flow rates. In order to widen the dynamic flow range, we designed a composite spring with two widths in serial (half of the turns are 9 μm thick, and the other half are 13 μm thick). The thinnest turns are located close to the anchor and the widest at the free end. Fig. 7 compares the flow-elongation characteristics of three different springs composed of 7 turns, two "homogenous" and one composite. At low Q the composite spring shows an elongation similar to that of an homogenous 9 μm width spring. Then the flow is sufficient to deform the turns with higher bending modulus, and all the turns elongate. At higher flow rates in the linear regime, the composite spring behaves like the homogenous 13 μm width spring. At intermediate flow rate, its elongation curve deviates from the linear behaviour at smaller flow rates than for the thin homogenous spring, and it finally merges with the curve from the thickest homogeneous spring, in the crossover region between linear and "pseudo-plateau" region. The measurable flow range of the heterogeneous spring is increased by one order of magnitude as compared to homogenous springs. Notably, the length in the "plateau" region at high flow rates continues to increase regularly. We interpret this as a consequence of the elongation of the spring's segments aligned along the flow. This elongation is reversible and measurable, and it contributes to extend the range of exploitable flow rates, for both the homogeneous and the non-homogeneous springs. For the latter, this range extends over 5 orders of magnitude (with maximal accuracy over 2 orders of magnitude). Also note that this extra contribution to the extension, associated with elastic elongation is stronger with the $w = 9$ μm spring, leading to an offset of the plateau towards higher lengths.

Conclusions

We demonstrated that microscope-based stop flow lithography allows the easy preparation of deformable microstructures inside microchannels, without any clean room equipment. These structures can be prepared with mechanical properties and dimensions reproducible to within better than 5%. We applied this technology to the preparation of spring-like flow sensors. These sensors can measure flow reversibly in a range of typically 4 orders of magnitude. The accuracy in the first two decades is around 3%. Accuracy decreases slightly in the upper range, but it remains better than 10%. It is worth mentioning that these performances were obtained in day-to-day experiments, in the research laboratory, on a microscope also used for other purposes. This tolerance could certainly be reduced much further in an industrial, automated and fully calibrated process. Note also that stop-flow lithography allows for the polymerization of micron sized structures, and that the resistance of the springs to rupture is very high (we could not achieve spring rupture even at the highest flow rates achievable with our syringe pump). So, we believe that the range of measurable flow rates could be shifted towards lower values by at least two orders of magnitude by reducing the dimensions of both the structures and the channel.

With an optimized design involving heterogeneous springs, measurable flow rate had been increased by one order of magnitude. This spring-based flow sensor requires a prior knowledge of the fluid's viscosity, in order to provide an absolute measurement of the flow. However, viscosity is an easy to measure property. Besides its ease of fabrication and fast prototyping, spring-based flow sensors are insensitive to the chemical content of the fluid if the viscosity is unchanged. This corresponds to many bioanalytical applications. This is a significant advantage as compared to sensors based on electrolysis, electrochemistry or thermal conduction. Also, this sensor does not require any specific tracer in the solution. It should thus be useful in many applications, in particular when flow sensing should be combined with other components in a single microfluidic chip. As a final notice, we used here imaging to measure the extension of the spring, but other detection means, such as AC impedancemetry with integrated electrodes could be easily contemplated, since PEGDA has a strong dielectric and conductivity contrast with water-based solutions.

Experimental

Materials

All photopolymerized structures shown in this work were prepared using 10% (w/w) solutions of Darocur 1173 (Sigma Aldrich) initiator in 50% (w/w) poly(ethylene glycol)(400) diacrylate (PEGDA, Polysciences) and 50% (w/w) poly(ethylene glycol)(700) diacrylate (PEGDA, Sigma-Aldrich). This ratio of PEGDA was chosen to yield maximal sensitivity of the sensor at the most practically useful flow rates.

All the springs were designed to have a width of 200 μm. The total length depended on the number of turns (typically 600 μm at rest for a 7 spires spring), and with a 70 μm circle built on at the end as an anchor surrounding the PDMS post in the microchannel. The spring was made of a series of straight sections joined by semicircular "hinges", with an external radius twice the width of the straight section. Under flow, most of the deformation is undergone by these hinges, progressively increasing their effective radius, and increasing the angle between the two contiguous straight sections. The illumination time (0.25 seconds) and the concentration ratios of polymer over photoinitiator were adjusted for the spring to elongate at the reachable flow rates (from 0.001 to 200 μl/min with our syringe pump).

The PDMS devices were fabricated by pouring polydimethylsiloxane (PDMS, Sylgard 184, Dow Corning) on a silicon wafer containing positive-relief channels patterned in SU-8 photoresist (Microchem). The devices were rectangular channels of 500 μm widths and 20 μm height, with 40 μm diameter posts every 4 mm. These devices were placed on glass slides spin-coated with PDMS to ensure that the pre-polymer was only contacted with PDMS surfaces. The formation and the deformations of the microsprings were visualized using a CCD camera (KP-M1EK-S10, Hitachi). Images were captured and processed using NIH Image software. The spring height was measured with an AMBIOS XP1 profilometer.

Photopolymerization setup

Photomasks were designed in AUTOCAD 2006 and printed using a 24000 dpi high-resolution printer at Selba S.A. (Versoix, Switzerland). The mask was then inserted into the field-stop of the microscope (Zeiss Axiovert 200, tube lens magnification 4×). A 100 W HBO mercury lamp served as the source of UV light. Objective magnification was a 10× (Zeiss Achroplan, 10X/0.25). A filter set allowing wide UV excitation (Excitation 365HT25, emission 400EFLP, Omega Opticals) was used to select light of the desired wavelength and a VS25 shutter system (Uniblitz) driven by a computer-controlled D122 shutter driver provided pulses of UV light with the specified duration. Solutions were driven through the microfluidic device with a Kd Scientific 210P syringe pump.

Acknowledgements

This work was supported in part by European project NeuroTAS under the NMP 6th framework program, and by ANR project "Polygen" under program TECSAN.

References

1 D. Dendukuri, S. S. Gu, D. C. Pregibon, T. A. Hatton and P. S. Doyle, *Lab Chip*, 2007, **7**, 818–828.
2 G. M. Whitesides, *Nature*, 2006, **442**, 368–373.
3 C. Sotomayor Torres, in *Alternative Lithography Unleashing the Potentials of Nanotechnology*, Springer, 2003.
4 P. S. Waggoner and H. G. Craighead, *Lab Chip*, 2007, **7**, 1238–1255.
5 J. Fritz, M. K. Baller, H. P. Lang, H. Rothuizen, P. Vettiger, E. Meyer, H.-J. Guntherodt, Ch. Gerber and J. K. Gimzewski, *Science*, 2000, **288**, 316–318.
6 A. F. Doll, M. Wischke, A. Geipel, F. Goldschmidtboeing, O. Ruthmann, U. T. Hopt, H.-J. Schrag and P. Woias, *Sensors and Actuators A*, 2007, **139**, 203–209.
7 S. F. Bart, M. Mehregany, L. S. Tavrow, J. H. Lang and S. D. Senturia, *IEEE Transactions on Electron Devices*, 1992, **39**, 566–575.
8 H. M. Simms, C. M. Bowman and K. S. Anseth, *Biomaterials*, 2008, **29**, 2228–2236.
9 D. J. Beebe, J. S. Moore, J. M. Bauer, Q. Yu, R. H. Liu, C. Devadoss and B.-H. Jo, *Nature*, 2000, **404**, 588–590.
10 D. Dendukuri, D. C. Pregibon, J. Collins, T. A. Hatton and P. S. Doyle, *Nature Materials*, 2006, **5**, 365–369.
11 J. G. Santiago, S. T. Wereley, C. D. Meinhart, D. J. Beebe and R. J. Adrian, *Experiments in Fluids*, 1998, **25**, 316–319.
12 J. Collins and A. P. Lee, *Lab Chip*, 2004, **4**, 7–10.
13 J. S. Rossier, A. Schwarz, F. Reymond, R. Ferrigno, F. Bianchi and H. H. Girault, *Electrophoresis*, 1999, **20**, 727–31.
14 Daniel C. Pregibon, Mehmet Toner and Patrick S. Doyle, *Langmuir*, 2006, **22**, 5122–8.
15 Y. Wang, G. T. Salazar, J.-H. Pai, H. Shadpour, C. E. Sims and N. L. Allbritton, *Lab on a Chip*, 2008, **8**, 734–740.